Automatic Osteosarcoma Classification System Based Multilayer Grid XG Boost Architecture

karthicsonia B (karthicsoniaramesh1@gmail.com)
Alagappa University https://orcid.org/0000-0002-7226-6495
M. Vanitha
Alagappa University

Research Article

Keywords: Osteosarcoma, Curvature based Anisotropic filter, Contrast Limited stretch Histogram Equalization, Contour based threshold segmentation, Stochastic linear embedding, Multilayer grid XG Boost

Posted Date: February 25th, 2022

DOI: https://doi.org/10.21203/rs.3.rs-1360315/v1

AUTOMATIC OSTEOSARCOMA CLASSIFICATION SYSTEM BASED MULTILAYER GRID XG BOOST ARCHITECTURE

B.Karthicsonia[1], Dr. M.Vanitha[2]

1.Research scholar, Dept of Computer Applications, Alagappa University, Karaikudi, India.

Karthicsoniaramesh1@gmail.com

2.Asst professor, Dept of Computer Applications, Alagappa University, Karaikudi, India.

mvanitharavi@gmail.com

Abstract

Osteosarcoma is the most frequent primary malignant bone tumour. Computer-aided detection (CAD) and diagnosis are being used to enhance osteosarcoma detection and diagnosis . The use of machine learning and deep learning algorithms may save up surgeons' time while also improving patient outcomes. An enormous quantity of data must be fed into the classifier for it to become more accurate. Adapted to a public dataset of osteosarcoma histology pictures, a mix of machine and deep learning is used in this work to distinguish between necrotic and healthy tissue images. First, the dataset was preprocessed, and contour based threshold segmentation techniques are applied. Then, Stochastic linear embedding based Feature extraction is used for extracting the abnormal features. Finally, the proposed multilayer grid XG Boost classifier is trained on stained images in order to increase the output accuracy. The experimental findings indicate that the proposed classifier has the greatest accuracy of any illness classification approach currently available. Our fine-tuned model showed superior performance in identifying osteosarcoma malignancy using H and E stained pictures.

Keywords: Osteosarcoma, Curvature based Anisotropic filter, Contrast Limited stretch Histogram Equalization, Contour based threshold segmentation, Stochastic linear embedding, Multilayer grid XG Boost

I. INTRODUCTION

Of all new pediatric cancer diagnoses, 5-10% are attributed to primary bone tumours. Among malignant primary bone tumours, osteosarcoma is the most often occurring kind. A difficult problem exists in the prognosis of osteosarcoma despite the fact that there are only around 1,000 new cases each year in the United States. In patients, the incidence is highest in children under the age of 10 and in teenagers between the ages of 10 and 20. Approximately 40 to 50 percent of all osteosarcoma cancer cases develop in the metaphysic of long bones in the lower extremities. There may be modest localized bone pain, redness, and warmth at the tumour location when osteosarcoma is first diagnosed. Increased discomfort limits patients' ability to move and use their joints. If osteosarcoma is not treated in its early stages, it may spread to the lungs, other bones, and soft tissues. Osteosarcoma diagnosis relies on biopsies, X-rays, and magnetic resonance imaging. For the time being, osteosarcoma diagnosis is made by a combination of medical history and physical examination. The most common signs and symptoms are swelling and persistent, deep-seated agony that feels like it's chewing at you. Because widespread pain may be a sign of bone metastases, it is important to have it checked out as soon as possible Standard studies for osteosarcoma evaluation include laboratory tests, an X-ray of the entire affected bone, an MRI of the entire affected bone, a chest X-ray, a chest computed tomography (CT) scan, and a whole-

body technetium bone scan with a percutaneous image-guided biopsy in addition to the examination. Despite the fact that biopsy-based approaches are very successful in detecting malignancy, histological guided biopsies and MRI scans have restricted their ability for detection. It takes time to prepare histology specimens as well. For example, to accurately diagnose osteosarcoma malignancy, at least 50 histology slides must be prepared to simulate a three-dimensional plane of a big tumour. There is an increase in the prevalence of cancer and patient-specific therapy choices, which makes cancer diagnosis and treatment more difficult. In order to thoroughly examine all of the slides, pathologists are needed to put in a lot of time. Histological pictures may be difficult to decipher because of their inherent subtleties. Inaccurate diagnoses are common as a result of the amount of labor required to make a diagnosis. Due to the similarity in osteoblast shape, it is difficult to tell them apart in a photograph. Additionally, a biopsy is a critical yet time-consuming step in detecting cancerous tissue. While this is going on, CAD technology provides radiologists with a way to automatically diagnose malignancies without the need of a human eye or a trained technician. Recent advances in cancer detection have relied heavily on microscopic image-based analysis to overcome these drawbacks. However, because to its poor detection accuracy, it was impractical prior to the 2000s. Clinical deployment was impossible due to CAD's low performance until recent improvements in computerized image detection. Advances in technology have made it possible to convert histology slides into digital image databases, where machine learning and deep learning may be used to improve digital pictures. Digital pathology is already a standard aspect of clinical diagnosis because to the development of whole slide imaging (WSI).. There are new opportunities to build new algorithms and software because of the rise of digital pathology. This technique allows for the quantification of a histological picture in order to enhance pathological operations. The technology digitizes stained tissue sections on glass slides at very high resolution pictures, making computerized image analysis feasible. In this research, the key objectives are:

1) To show that machine learning-based algorithms are capable of accurately diagnosing osteosarcoma malignancy using a publicly available dataset. In order to identify non-tumors, necrotic tumours, and cancer that is still alive, this research must be effective.

2) Investigate a suitable deep learning framework for effective detection and uncover potential hints that aid performance. It is necessary to apply segmentation and classification in a unique, substantial, practical, and efficient way that gives encouraging results in the classification of osteosarcoma images. We developed an efficient architecture for classifying input images into tumour classifications with fewer attributes by combining contour-based threshold segmentation with a multilayer grid XG Boost classifier. This has the dual benefits of saving both time and space. We also compare our suggested architecture's tumour classification results with those of current architectures to demonstrate that the proposed architecture is superior.. The remaining section of the paper can be organized as follows, Related works is briefly summarized in section 2.The problem statement was depicted in section 3. The suggested methods for brain tumor volume calculation was illustrated in section 4.The experimental results was presented in section 5. Finally section 6 concludes the work.

II. RELATED WORKS

[1] Using the SJTU team's metabolomic data on osteosarcoma patients, employ logistic regression, support vector machine (SVM), and random forest (RF). These devices are compared based on their receiver operating characteristic curves. All three classifiers can tell between tumours, however cross-validation tests using the training data show that random forest outperforms the others (accuracy rate for logistic regression, support vector machine and random forest are 88 percent , 90 percent and 97 percent respectively). Random forest had a 95% overall accuracy rate with a 0.99% AUC on the testing set . [2] Considering modest numbers of histological osteosarcoma, a Sequential Recurrent Convolutional Neural Network (RCNN) model combining CNN with bidirectional Gated Recurrent Units (GRU) is developed. Imagery stained with Haematoxylin and Eosin (H & E)

despite the over-fitting issue, heterogeneity, and noisy data . [3] Pre-trained CNNs can distinguish between necrotic and non-necrotic tissue using transfer learning methodologies in a publicly available dataset of osteosarcoma histology images. Data was preprocessed and categorised in a variety of ways at the outset of the project. A transfer learning model such as VGG19 or Inception V3 is used to increase the accuracy of the outputs after they have been trained on Whole Slide Images (WSI). As a result, they're put to good use in binary and multi-class classifiers . [4] Propose a deep collaborative learning-based computer approach for identifying lncRNA-disease associations. (LDICDL). An automatic encoder indicates the presence of several lncRNA characteristics as well as information on different disease features. The lncRNA-disease associations may then be predicted using the matrix decomposition approach. Besides predicting associations between new lncRNA (or sickness) and illnesses, the hybrid model is also built to counteract the decline in matrix decomposition (or lncRNA). [5] DS-Net constructed on full convolution network serves as an auxiliary supervision network (ASN) and classification network (CN) in this case. With the Siamese network-based ASN, the problem of a small training set will be solved (the main bottleneck of deep learning in medical images). Coupling of labels is used to input and update the network using paired data in the input. The classification network makes use of the ASN-extremely accurate classification functions for its classifications . [6] radiomics research looking at diagnosis, treatment response, and patient survival for people with osteosarcoma should be assessed for methodological quality and bias . [7] 18F-FDG PET was used to conduct baseline and post-chemotherapy assessments, and the Chang-Gung Image Texture Analysis toolkit was used to assess 18F-FDG textural characteristics. The principle component analysis (PCA) feature selection approach was used to choose numerous characteristics to predict the chemotherapeutic response. SVM, random forest, and gradient boost algorithms were used in the machine learning process . [8] create machine learning-based CT radiomic characteristics to identify individuals who will progress to metastatic disease after being diagnosed with osteosarcoma. [9] MRN has been introduced here for osteosarcoma image segmentation for repeated monitoring of the residual network. Three supervised side output modules made up the remainder of the network. When using the shallow module, you may get information like edge features and texture attributes. Semantine attributes may be retrieved from the deep side module output. It's possible that the side output module will compute and disseminate information about the loss based on the difference in probability maps between the output and the ground. The remaining network parameters may then be altered using a gradient descent technique. This may serve as guidance for the network's multi-scale learning. The final segmentation results were acquired by the merging of data from the three side output modules. [10] improve the accuracy of pre-treatment MRI radiomics in forecasting chemotherapy response. [11] developed a strategy for differentiating tumour from exosomal host response mRNA produced by canine osteosarcoma xenografts in mice. A bioinformatic technique that uses RNA sequencing and species discrimination may be used to find gene signatures unique to canine osteosarcoma using this method . [12] Propose a strategy for multi-threshold fragmentation based on the modified algorithm salp swarm (SSA). The approach of multi-threshold fragmentation has a significant influence on segmentation, however the increase in threshold numbers reduces the accuracy of segmentation . [13] Long non-coding RNA (lncRNA) and autophagy were shown to be associated with osteosarcoma patient prognosis using bioinformatics tools and machine learning methodologies . [14] by using DNA methylation and transcription data from patients with OS, a comprehensive investigation was undertaken to identify the best lncRNA signature methylated for predicting OS prognosis. For therapeutically relevant studies, the original OS data sets were retrieved from the TARGET database. Patients that survived OS were found using Univariates, Lasso, and machine learning techniques in combination with Lasso Cox regression analysis. The Kaplan-Meier curves and Recipient Operating Feature (ROC) were used in this signature to determine whether or not the message was genuine. For OS patients, they devised a mechanised lncRNA signature that might help predict survival (verified in independent cohort [GSE39055]). According to Kaplan-Meier research, the signature can tell the difference between persons who are at high risk of death and those who are not . [15] improve osteosarcoma detection and

diagnosis using computer-aided design and diagnostics (CADx). By using instruments like CNNs, the operator's workload is reduced, and patient predicting is improved. The more data fed into a CNN, the more confident it will perform. For tailoring necrotic pictures to public osteosarcoma histology datasets, they use transmission methods and prequalified CNNs trained on healthy and non-necrotic tissues. The initial phase included preparing the data and applying several classifications to the collection of information. By training whole slide pictures, we may improve output accuracy (WSI). The transfer models, such as VPG19 and Inception V3, will be utilized if there are no patches. Final application is to binary and multi-class classification problems, where the models are used . [16] they propose the use of a convolutional neural network for the faster and more accurate classification of Osteosarcoma tumours into tumour classifications (live tumour, necrosis) (CNN).

III. PROBLEM STATEMENT

More over 80 percent of the world's poor and growing economies are affected by osteosarcoma. To ensure accurate OS measurements and analysis, Hand E images are critical in the clinical evaluation procedure. When osteo sarcoma is in its early stages, patients may have no symptoms at all. When a tumour grows, it's possible that a bulge or swelling may occur on the skin. Tumors may impair mobility or irritate nearby nerves, causing tingling, numbness, or other unpleasant sensations. In some cases, the symptoms of osteo sarcoma are mistaken for those of arthritis or other non-cancerous diseases that cause inflammation, such as bursitis, and are not linked to cancer. As a consequence, an accurate method of detecting Osteosarcoma at an early stage is necessary.

IV. PROPOSED WORK

Figure1 summarizes the proposed framework. This framework demonstrates an improvement over past efforts. It represents the components of a process that can be implemented for the operation of the osteosarcoma prediction.

The whole experiment was carried out in the cancer imaging archive as a dataset. The collection includes images of osteosarcoma histology taken with a hematoxylin and eosin stain (H&E). As a result of this, the data set includes 1144 pictures of the same size at 1024 X 1024 resolution and 10x resolution, comprising 536 pictures of non-tumors, 263 pictures of necrotic tumours, and 345 pictures of live tumours.

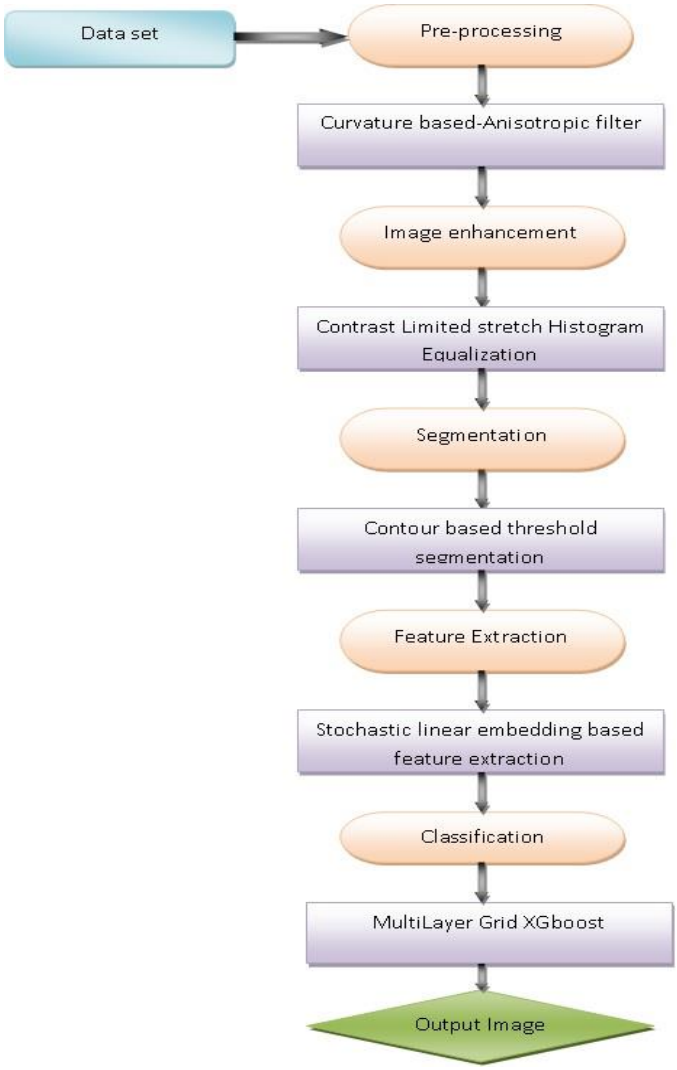

Figure 1 schematic representation of the suggested methodology

a.Pre-processing

An iterative approach for restoring the intensities in MR pictures is the anisotropic diffusion filter. These edge-stopping functions are utilized to accomplish what was previously only possible with the gaussian and gobel filters. The anisotropic diffusion filter, on the other hand, is significantly superior. An anisotropic diffusion filter, often known as an ADF, is a repeating algorithm that works by simulating the diffusion process in the following ways,

$$\frac{\partial D(x,y,t+1)}{\partial n} = div(\nabla D) \quad (1)$$

Here

$$D(x,y,t+1) = D(x,y,t) + div(H(|\nabla D|)\nabla D)$$

Where,

∂ = Noise filter

∇D = Summation of noise scores

x, y, t = noise Value of the Neighbor pixels,

n = Number of pixels in the image

Noisy pixels are filtered out considerably more quickly than edge pixels for two reasons in particular. The first is that, according to the equation, gradients in the opposite direction cancel out their effects, but this is not the case with noise pixels. Second, the anisotropic diffusion filter has an impact that is only substantial enough when there are a large number of neighbours with a high gradient magnitude. Noisy pixels are dispersed across the picture rather than being concentrated in one area, thus their intensity remains unique from that of the surrounding pixels.

$$M(x,y,F+1) = D(x,y,F) + \frac{\lambda}{|\eta_{(x,y)}|} \sum_{(i,j)\in\eta_{(x,y)}} H\left(\left|\nabla D_{(i,j)}^{(x,y)}\right|\right) \nabla D_{(i,j)}^{(x,y)} \quad (2)$$

Edge pixels, on the other hand, have a pixel signature that is considerably more comparable to that of the majority of the pixels in their vicinity. This aids in the removal of impurities that might make tumour identification more difficult in the future during morphological surgeries.

$$\nabla e_{90^\circ}^{(x,y)} = D(x,y-1,F) - D(x,y,F) \quad (3)$$

$$\nabla e_{-90^\circ}^{(x,y)} = D(x,y+1,F) - D(x,y,F) \quad (4)$$

$$\nabla e_{0^\circ}^{(x,y)} = D(x+1,y,F) - D(x,y,F) \quad (5)$$

$$\nabla e_{180^\circ}^{(x,y)} = D(x-1,y,F) - D(x,y,F) \quad (6)$$

Then after removal of the unwanted errors the histogram of the image can gets equalized by using the Contrast Limited stretch Histogram Equalization by which the image can be sharpened by using the stretch function,

$$W_{2^j}^{m,n}K(a,b,t+1) = W_{2^j}^{m,n}K(a,b,t) + \frac{\lambda}{|\eta(a,b)|}\sum_{(p,q)\in\eta(a,b)} h\left(\left|\nabla W_{2^j}^{m,n}K(a,b,t)\right|,\sigma\right)\left|\nabla W_{2^j}^{m,n}K(a,b,t)\right| \quad (7)$$

Where $\sigma = \sqrt{5\sigma}$ represents the simultaneous sharpening functions that be expressed as

$$P_{FBD}\ (W(i.j,k) = c_{FBD}\ (\|\nabla W\ (i,j,k)\|)\ \text{div}\ (\frac{\nabla W\ (i,j,k)}{\|\nabla W\ (i,j,k)\|}) \quad (8)$$

The enhancement form of the histogram can be represented as,

$$P_{FBD}\ (W(i.j,k) = \text{f}(g_{FBD}\ (W(i.j) - \ (W(i.j,k)) \quad (9)$$

The sharpening function can be represented as,

$$contrast = \sum_{i,j=0}^{F-1} P_{ij}(i-j)^2 \quad (10)$$

The above expression can sharpen the input signal.

b.Segmentation

Segmentation is an essential step in the processing of images. In this method, an object is detected by grouping similar pixels. It is employed for the extraction of the abnormal area in the images in which the preprocessed image can be given as a input. The raw input images are converted into measurable representative types and relevant details are extracated from it that assist in the diagnosis of the osteosarcoma. The area of the abnormality was pointed out and the approximate distance over the abnormality. The abnormal probability value calculated by using the formula as,

$$P(b_g) = \frac{N(b_g)}{Q} \quad (11)$$

The probability area value helps to improve the pixel capacity among the edges. A contour based threshold segmentation aim is to maximize the pixel capacity with minimum time by selecting the suitable threshold and the equation as follows,

$$Edge_g = \begin{cases} \min(I_{inj_n}), & if\ g = 0 \\ Edge_{g-1} + \Delta\omega, & if\ g = 1,2,\dots m \end{cases}$$

$$I_{inj_n}(i,j) \in b_g\ , if Edge_{g-1} \leq\ I_{inj_n}(i,j) < Edge_g \quad (12)$$

The equation can be rewritten as,

$$Edge_g = \max_{cc}\ Contour\ \frac{N_c(T_g|+T)_{f*M*S_c}}{T} * \log_2(1+\frac{\delta TP}{N_0.S_c}) \quad (13)$$

Here $\Delta\omega = \text{maxcc}\ \frac{N_c(T_g|+T)_{f*M*S_c}}{T}$

Where,

N_c as spacing of pixels

S_c as number of edges

T_g as pixel intensity

f as frequency threshold among the pixels

For each pixel in the image, a threshold has to be calculated. The threshold for each single pixel is found by interpolating the results of the sub images that can be depicted as,

$$\omega_g = N(b_g)^f \quad (14)$$

$$Edge_g^{'} = \begin{cases} 0, & if\ g = 0 \\ Edge_g^{'} + \frac{\omega_g{'}}{\sum \omega_g{'}} & if\ g = 1,2, \dots m \end{cases} \quad (15)$$

According to the methodology the abnormal area and the background region are divided. Let T_g^{JND} and $\omega_g{'}$ indicate the background and the abnormal area, they can be computed as,

$$T_g^{JND} = \sum \mu_1 \omega_g \times \mu_2 \frac{\Delta L_g}{\sum L_g} t_1 * \overline{t_2} \quad (16)$$

$$\omega_g{'} = \begin{cases} \omega_g & if\ \omega_g \le T_g^{JND} \\ T_g\ , otherwise \end{cases} \quad (17)$$

Where, g is the pixel value,

$\overline{t_1}$ and $\overline{t_2}$ is the means of the threshold of an image

μ_1 and μ_2 is the standard deviations of the pixel

The priori probabilities of the H and E image are presented as P (R) and P (S). Let $P_f(t)$ be the PDF of the image I_f , and it can be calculated as

$$P_f(t) = P(R)\, Ps(t) + P(S)\, P_l(t) \quad (18)$$

To enable the segmentation by the threshold σ_1 satisfies P (R) $Ps(\sigma_1)$ = P (S)$P_l(\sigma_1)$ and the formula as given below:

$$\text{Binary } (a,b) = 0,\ I_f(a, b) < \sigma_1 1,\ I_f(a, b) < \sigma_1 \quad (19)$$

Where (a, b) is the pixel location

I_f (a, b) is the pixel value of (a, b).

In general, the threshold σ_1 never computed since $P_s(t)$, $P_l(t)$, and the priori probability of each class in the image are unknown. Hence, σ_1 gets approximated by the global local minima that eliminate the fluctuations after segmentation on the PDF. It is possible to get the adaptive global threshold by finding the global local minima for segmentation. By enabling the images' binary threshold, the final threshold value is calculated for better segmentation based on characteristics.

The threshold is based on the arithmetic mean of the intensities of all nonzero pixels. The threshold (T) may be calculated using the equation below:

$$T_c(i,j) = \left(\frac{HW_c(i,j)}{y_{in}(i,j)}\right)^S . \gamma_{out}(i,j) \quad (20)$$

$$D_{inj}(i,j) = 10^{\tau(i,j)}$$

Where, h and W are the height and width of the image (I) respectively. Finally the tumor map can gets calculated will sort out the abnormal area.

c.Feature extraction

The stochastic linear embedding based Feature extraction

for Feature Extraction may be employed for the extraction of the specialized functions for classification. Feature Reduce Framework offers optimistic results and helps in the processing of huge data by distributing data as tiny portions of clusters. The large volume of data is segregated into subgroups, and interrelationships need to be evaluated to avoid major problems, while adding the resulting data leads to structured data development. The data must be grouped according to its data and size. The own values can be determined after clustering. Determines the Eigen co-variance matrix vectors and project the data into a new subspace equal or less scaled by using these patented vectors. The correlation or co-variance data matrix is usually generated by the calculation of the automated vector matrix. The subset of variables from a large dataset is chosen based on real variables with optimum similarity with the main component.

$$e(W) = f(t)\sum_{i=1}^{n}\left\|x_i - \sum_{j=1}^{n} w_{ij}x_j\right\|^2 \frac{\lambda_1+\lambda_2+\lambda_3.....\lambda_k}{\lambda_1+\lambda_2+.....+\lambda_k+.....\lambda_d} \quad (21)$$

λ is the Eigenvalue; w is the new set of features; x is the original features

Where $f(t) = A_L + \sum_{j=1}^{L} H_j, \sum_{j=1}^{n} w_{ij} = 1$ (22)

$$A = diag\ (\lambda_1, \lambda_2, \ldots\ldots \lambda_m) \quad (23)$$

Here, A defines the diagonal matrix of Eigen values. We need to approximate mainly n eigenvectors that lead to the largest Eigen values to reflect the data records with low dimensional vectors, $\phi = l_1,\ l, \ldots\ldots\ l_m$

$$\phi(Q) = \sum_{i=1}^{n}\left\|q_i - \sum_{j=1}^{n} w_{ij}q_j\right\|^2 \quad (24)$$

Where$\sum_{i=1}^{n} q_i = 0,$

$$\frac{1}{N}\sum_{i=1}^{n} q_i q_i^T = I \quad (25)$$

$$Q = [v_2, \ldots. v_{d+1}]^T \quad (26)$$

Then determine the number of features by using the following criterion,

$$\frac{\sum_{u=1}^{T}\lambda_i}{\sum_{u=1}^{P}\lambda_i} > M \quad (27)$$

P is the total number of Eigen feature vectors.

The basic equation of these features is discussed below.

(i) Mean (m)

$$m = \frac{1}{l}\sum_{i=1}^{l} X_i \quad (28)$$

(ii) Standard deviation (sd)

$$sd = \sqrt{\frac{1}{l-1}}\sum_{i=1}^{N}(X_i - m)^2 \quad (29)$$

(iii) Edging feature

$$e = \sum_{i=1}^{N} X_i^2 log X_i^2 \quad (30)$$

(iv) Skewness feature (skw)

$$skw = \frac{1}{l}\sum_{i=1}^{l}\left[\frac{X_i - m}{sd}\right]^3 \quad (31)$$

d.Classification

It uses a gradient-boosting framework which is based on decision-tree-based algorithm . In XGBoost the learning methods are strengthened by using ensemble tree approaches. The common boosting classifier in which it divides the values in accordance with the hyper-parameter max-depth set and then starts the reversing pruning of the tree and deletes breaks below that and no positive gain is achieved. Since a split that does not minimize loss is commonly followed by a split that does minimize loss, this multilayer grid XGBoost method is used.

$$\varepsilon_{maf}(\phi, f1, f2) =$$
$$\lambda_1 \iint_{\Omega} N_\sigma(x-y)|I(y) - f1(x)^2 H(\phi(y)dydx +$$
$$\lambda_2 \iint_{\Omega} N_\sigma(x-y)|I(y) - f2(x)^2\big(1 - H(\phi(y)\big)dydx$$
$$\lambda_1, \lambda_2 > 0 \quad (32)$$

There is an additional regularization term added to balance the model's complexity with the declining loss function that is used by the suggested classifier. It aims to find the best overall answer while avoiding excessive tailoring. In order to speed up and enhance algorithm accuracy, XGboot uses a multi-threaded Processor to conduct gradient tree boosting techniques in parallel. Because XGBoost is a boosting technique based on residuals, let's assume the model contains x decision trees.

$$D = \{x: \phi(x) = 0\} \quad (33)$$

$$\Omega_1 = \{x: \phi(x) > 0\} \quad (34)$$

$$\Omega_2 = \{x: \phi(x) < 0\} \quad (35)$$

The loss function can be represented as,

$$I(x) = \frac{1}{2}\left[1 + \frac{2}{\pi} arctan\left(\frac{x}{\epsilon}\right)\right] \quad (36)$$

This modifications are made from the result obtained from the decision trees involved in the classifier. These revisions take the ranking process. The steps concerned some of the parameters include inputs, outputs and errors. which can be represented by equation,

$$i = /(1 + \left|\delta G_{\xi} * J\right|^2) \quad (37)$$

$$\varepsilon_{i(\phi)} = \int_{\Omega} i\delta(\phi)|\phi|dx \quad (38)$$

Where i is a functional matrix , δ is the classifier of the dual variables,

$$\mathcal{F}(\phi, f1, f2) \quad (39)$$

$$\frac{\partial \phi}{\partial t} = \frac{\partial \mathcal{F}}{\partial \phi} \quad (40)$$

Next, a set of rules will construct a selection tree for every sample. Then it'll get the prediction result from each decision tree.

$$\frac{\partial \phi}{\partial t} rule\ 1 = -\delta\ (\phi)(\lambda_1 e_1 - \lambda_2 e_2) + v\delta(\phi) div\left(i\frac{\phi}{|\phi|}\right) \quad (41)$$

Where $\delta\ (x) = \frac{1}{\pi}\frac{\epsilon}{\epsilon^2 + x^2}$

$$\delta\ (x) rule\ 2 = \frac{\partial \phi}{\partial t} = -\delta\ (\phi)(\lambda_1 e_1 - \lambda_2 e_2) + v\delta(\phi) div\left(i\frac{\phi}{|\phi|}\right) + \left[a^2\phi - div\left(\frac{\phi}{|\phi|}\right)\right]$$

(42)

In this step, voting will be performed for every predicted result.

$$\begin{cases} e_1(x) = \int_{\Omega} N_{\sigma}(y - x)|I(x) - f1(y)^2 dy \\ e_2(x) = \int_{\Omega} N_{\sigma}(y - x)|I(x) - f2(y)^2 dy \end{cases} \quad (43)$$

Finally, a ranking is generated for the abnormality matching distance of data base datas,

$$JS = \frac{R_S \cap T_S}{R_S \cup T_S}, \quad (44)$$

Where R represents the rank and T represents the total data

The classification was concluded as

$$Classification = \left|\frac{R_S - T_S}{R_S}\right| \quad (45)$$

Algorithm: 1 (Multilayer grid XG Boost)

Input: Extracted features

Output: Classified output

Initialize all the parameters.

$$P(b_g) = \frac{N(b_g)}{Q}$$

Point abnormality(#) flag

$$T_c(i,j) = \left(\frac{HW_c(i,j)}{y_{in}(i,j)}\right)^S . \gamma_{out}(i,j) \quad (20)$$

$$D_{inj}(i,j) = 10^{\tau(i,j)}$$

Segment image

End

For

Feature map analysis,

Mean (m)

$$m = \frac{1}{l}\sum_{i=1}^{l} X_i$$

Standard deviation (sd)

$$sd = \sqrt{\frac{1}{l-1}}\sum_{i=1}^{N}(X_i - m)^2$$

Edging feature

$$e = \sum_{i=1}^{N} X_i^2 log X_i^2$$

Skewness feature (skw)

$$skw = \frac{1}{l}\sum_{i=1}^{l}\left[\frac{X_i - m}{sd}\right]^3$$

Classified data(flag)

Train,test data (70,30)

$$\begin{cases} e_1(x) = \int_\Omega N_\sigma(y-x)|I(x) - f1(y)^2 dy \\ e_2(x) = \int_\Omega N_\sigma(y-x)|I(x) - f2(y)^2 dy \end{cases}$$

Voting and ranking

For

End

$$Classification = \left|\frac{R_s - T_s}{R_s}\right|$$

Set classification.status = Normal

Else

Set Node.status = abnormal

return

End

End

V. PERFORMANCE ANALYSIS

The proposed method is simulated using the MATLAB simulation tool. The behavior of the suggested technique is validated concerning the specifications like accuracy, precision, F1 score and recall. Four concepts are to be considered for this evaluation: True Positive (TP), True Negative (TN), False Positive (FP), and False Negative (FN). TP is defined as the pixel numbers that are detected accurately as positive by the algorithm. TN is defined as the pixel numbers, which are detected accurately as negative by the algorithm. FP is defined as the pixel numbers that are detected as positive but not the exact ones. FN is defined as the pixel numbers that are detected as negative but not the exact ones.

- TP means osteosarcoma is present

- TN means osteosarcoma is not present and is not identified.
- FP means osteosarcoma is not present but is identified.
- FN meansblack fungusis present but is not identified.

We also contrast the suggestedtechnique with a few of the existing techniques concerning these parameters.

$$Accuracy = \frac{True\ Positive+True\ Negative}{True\ Positive+False\ Negative+False\ Positive+True\ Negative} \quad (46)$$

$$Precision = \frac{True\ Positive}{True\ Positive+False\ Positive} \quad (47)$$

$$Recall = \frac{True\ Positive}{True\ Positive+False\ Negative} \quad (48)$$

$$F_1 = \frac{2*Precision*Recall}{Precision+Recall} \quad (49)$$

$$TPR = \frac{True\ Positive}{True\ Positive+False\ Negative} \quad (50)$$

$$FPR = \frac{False\ Postive}{False\ Positive+True\ Negative} \quad (51)$$

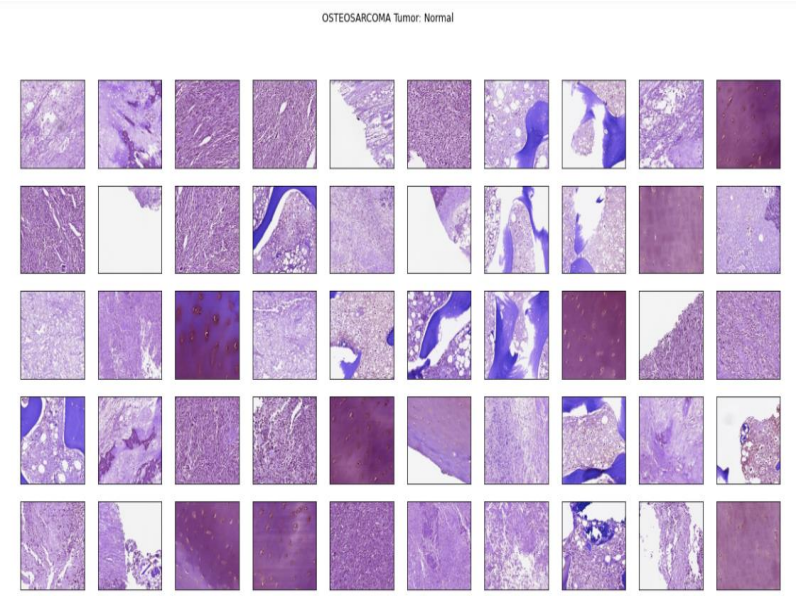

Figure (2a)

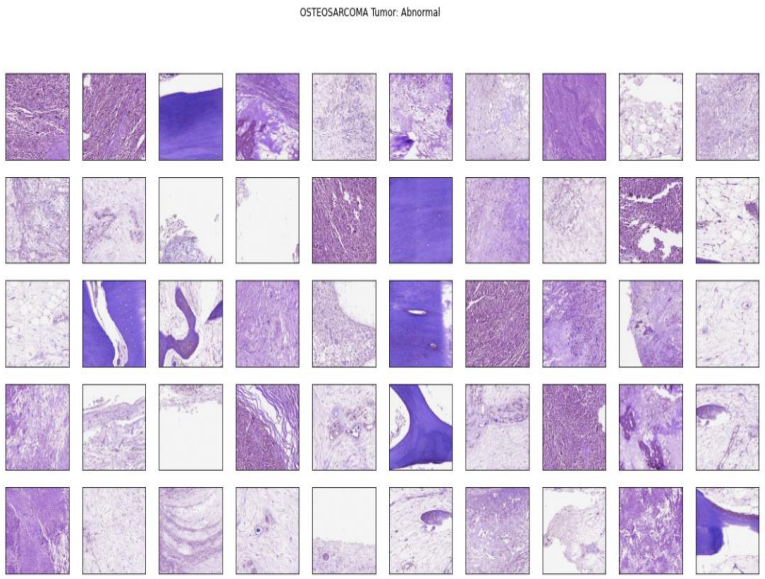

Figure (2b) Classified output

Classifying input picture tiles into normal and abnormal (live tumour, coagulative necrosis, osteoid or fibrotic tissue, non-tumor) was the goal of thesuggested classifier. The classifier's output is a probability distribution with a total of 1. Here as of from figure 2(a,b) the suggested classifier can accurately classifies the normal and the abnormal images. To prove the effectiveness of the suggested classifier it can be run along with the common existing CNN and XG boost.

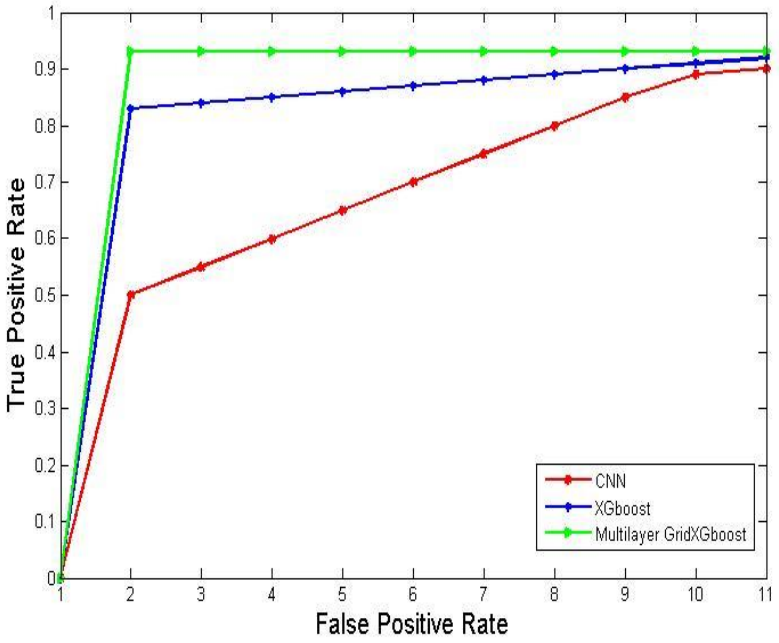

Figure 3 ROC for normal and Necrotic tumor

Figure 3,4,5,6 shows that among all the classifications, multilayer grid XG Boost has the greatest AUC with ROC value. As we can see from the ROC and AUC values (0.95 for non tumor vs necrotic tumour, 0.96 for viability against non-tumor, 0.98 for

necrotic tumour versus non-tumor, and 0.92 for viability versus non-tumor), there is a high degree of predictability. As a result of the above analysis, we can safely state that multilayer grid XG Boost is effective across all categories.

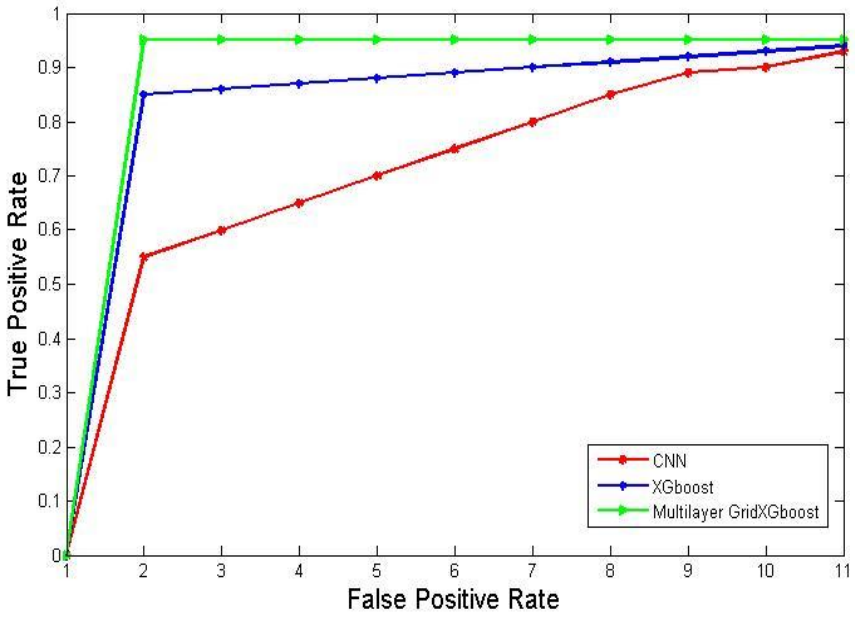

Figure 4 ROC for normal and viable tumor

As of from figure 4 the suggested classifier acquires high range of ROC over normal Vs. viable tumor.

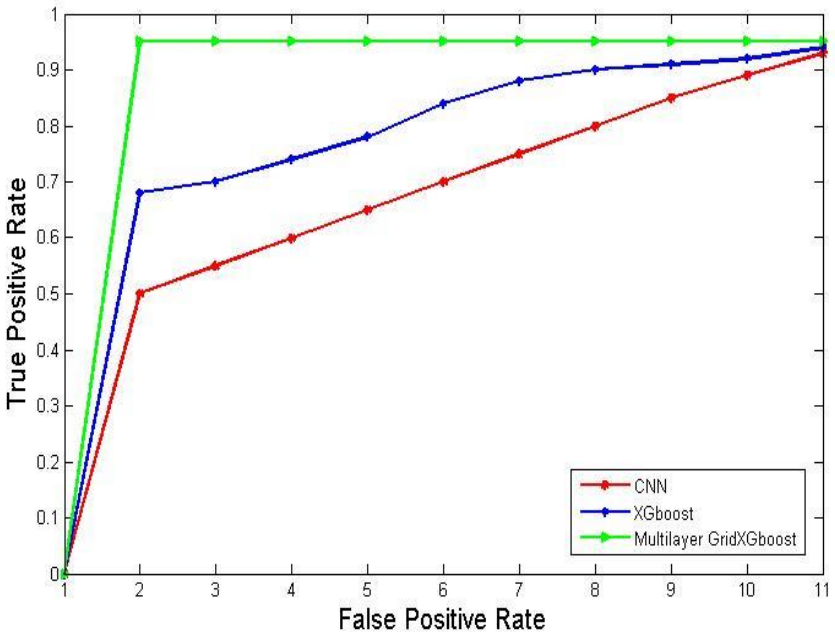

Figure 5 AUC for normal and necrotic tumor

As of from figure 5 the suggested classifier acquires high range of AUC over normal Vs. necrotic tumor.

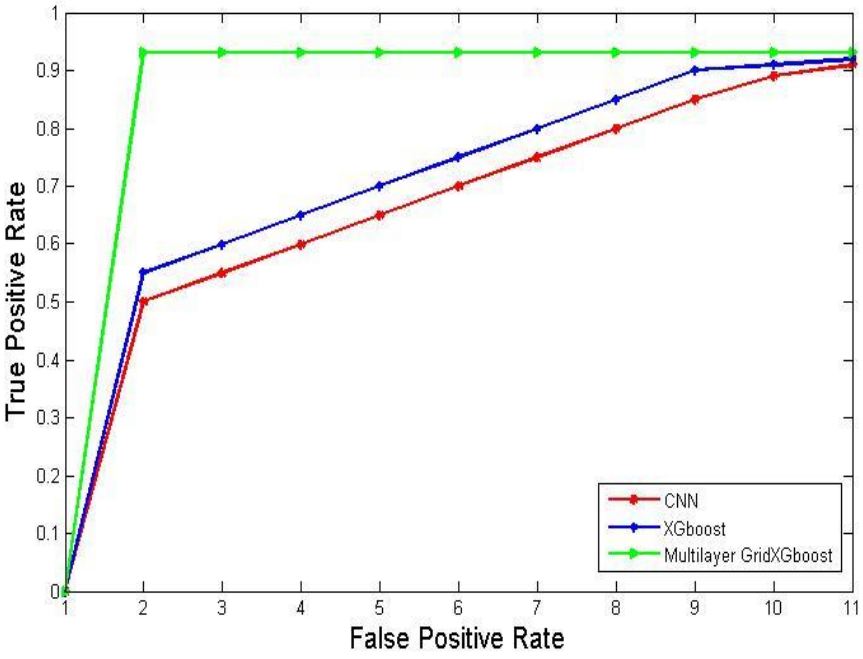

Figure 6 AUC for normal and viable tumor

As of from figure 6 the suggested classifier acquires high range of AUC over normal Vs. viable tumor.

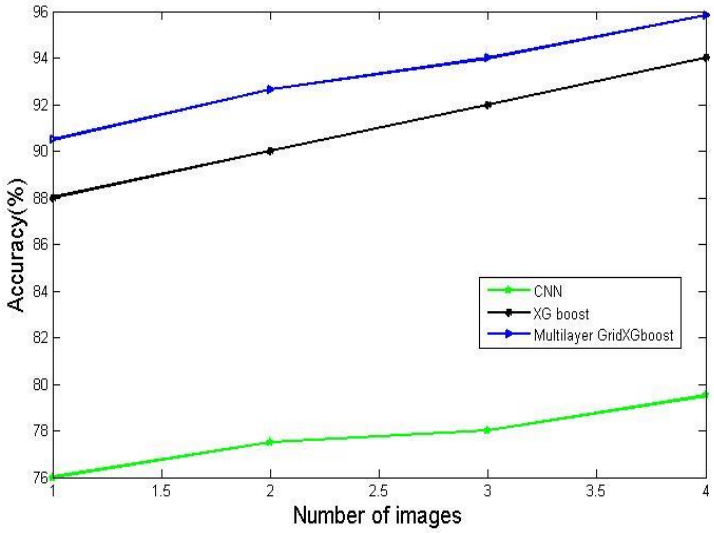

Figure 7 Number of images Vs. Accuracy

Figure 7 shows the proposed classification method, showing a maximum accuracy yield of 96%, which is better than CNN (79.9) and XG boost(93%).

Hence among the three classifier the multilayer grid XG boost expressed satisfied results than other two classifiers. To prove the efficiency of the multilayer grid XG boost it can be compared with the [16] existing methodology.

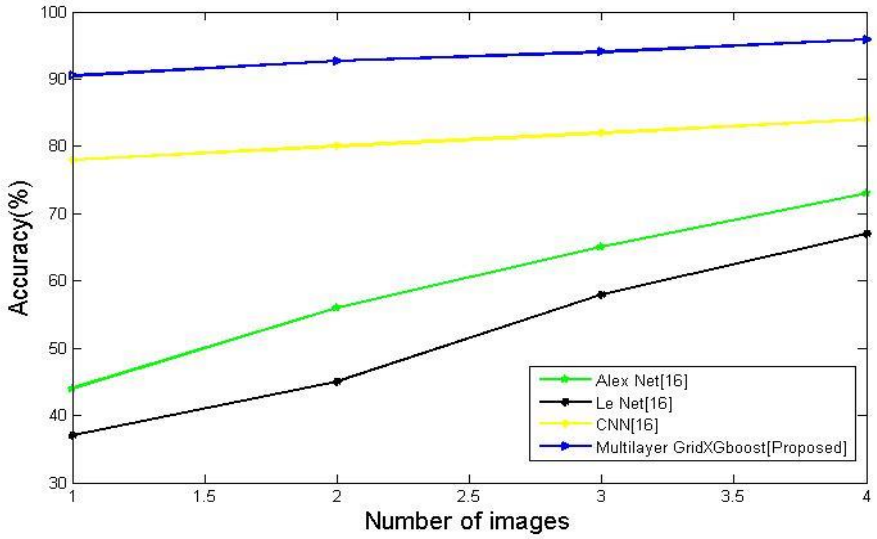

Figure 8 Number of images Vs. Accuracy percentile

Figure 8 shows the results of accuracy between the proposed multilayer grid XG boost with existing methods. The result shows that osteosarcoma computation burden using the proposed method has reduced to a greater extent than the other methods in state of prediction accuracy.

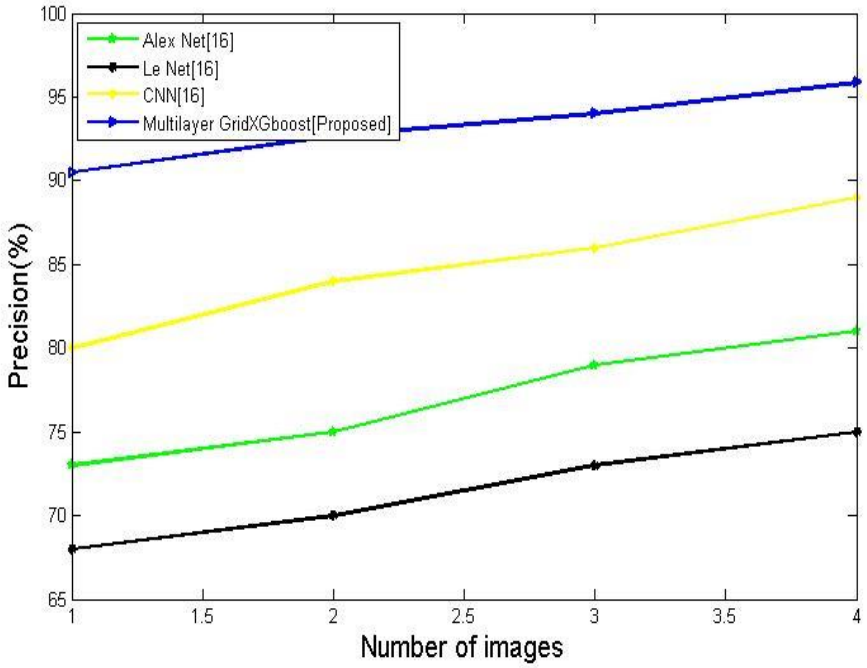

Figure 9 Number of images Vs. Precision

Figure 9 graph shows the proposed system which shows a higher precision rate (96%) when compared with the system already in use**.**

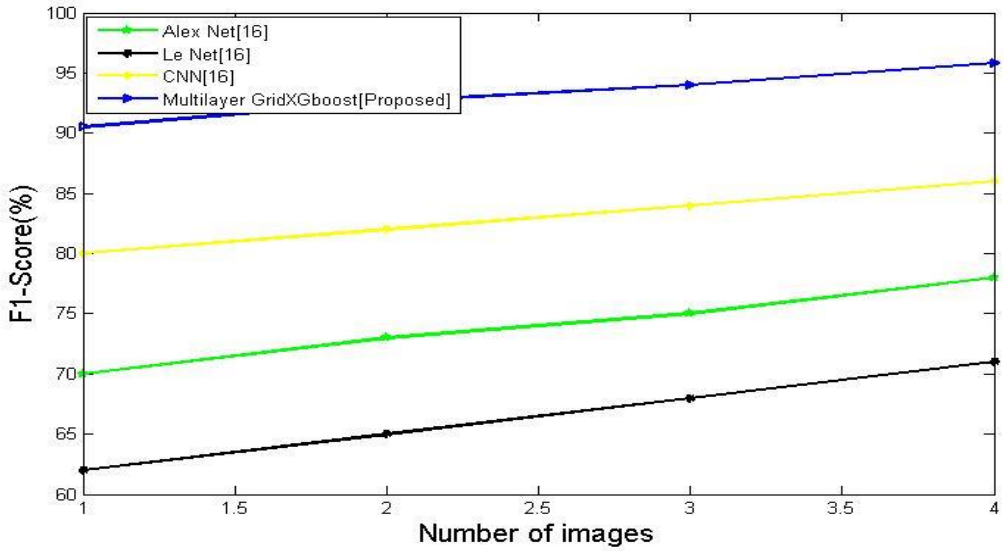

Figure 10 Number of images Vs. F1 score

For the solution, figure 10 is a F1 ranking. The findings reveal that, the proposed method shows exact high values regarding coefficient of F1 score which was 96%.

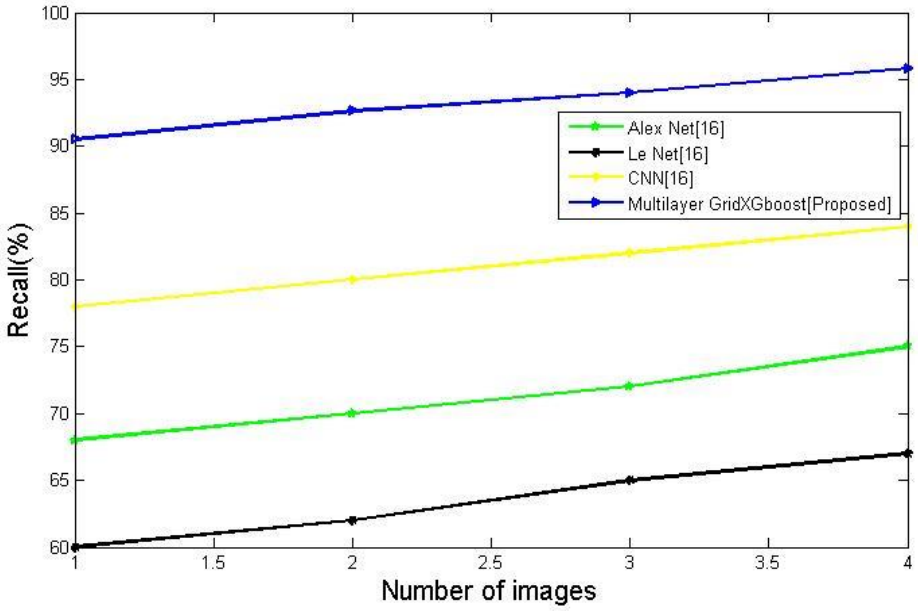

Figure 11 Number of images Vs. Recall

Figure 11 shows the proposed classification method, showing a maximum recall yield of 96%, which is better than conventional methods. To prove the efficiency of the suggested classifier performance it can be compared with some other existing methodologies [17] .

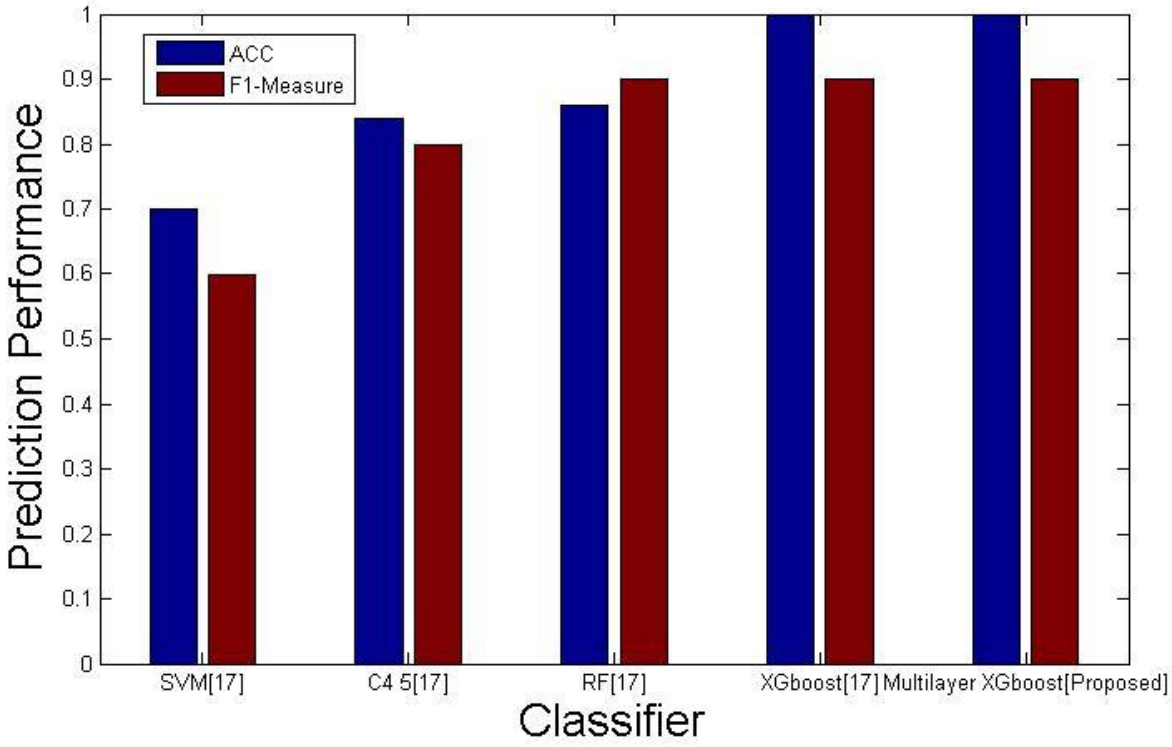

Figure 12 Performance prediction of the classifiers

Figure 12 depicts the performance scores of five classifiers for two performance criteria in a more understandable way (more intuitively). Under the performance measures, multilayer grid XGBoost has the best performance, whereas SVM has the poorest. From the result obtained it was revealed that the suggested classifier express satisfied result than other existing methodology.

VI. CONCLUSION

Using computer-aided methods to classify histology pictures has become more significant in medical image processing. A microscopic inspection of histological pictures is complex and time consuming. The use of automated histology diagnosis reduces pathologists' workload, allowing them to devote more time to high-priority cases. In this paper a new Segmentor with machine learning based Classifier was developed and applied to increase classification accuracy for Osteo sarcoma prediction. In fact, new statistical methods for the diagnosis of Osteosarcoma are being applied. By using the proposed abnormality classification classifier, better classification accuracy (96%) can be obtained. On the other hand, in binary class, the Necrotic Tumor against Non-Tumor received an F1 score of 0.96.When comparing our results to those of the prior research using the identical data, we came out on top in both the binary and multi-class categories. To validate the proposed model, the analysis was conducted using the cancer imaging archive database.

Acknowledgements:

This work has been supported by RUSA PHASE 2.0 Alagappa University , Karaikudi.

Author contributions:

B.Karthicsonia: validation and visualization, Investigation and methodology, Writing original draft .

Dr.M.Vanitha: validation and visualization, Writing –review and editing

All the authors' have read and agreed to the publication of this manuscript.

Compliance with ethical standards

Conflict of interest: The authors declare that they have no known competing financial interests or personal relationships that could have appeared to influence the work reported in this paper.

REFERENCES

[1] Z. Li, S. R. Soroushmehr, Y. Hua, M. Mao, Y. Qiu, and K. Najarian, "Classifying osteosarcoma patients using machine learning approaches," in *2017 39th Annual International Conference of the IEEE Engineering in Medicine and Biology Society (EMBC)*, 2017, pp. 82-85.

[2] M. Rahad Arman Nabid, L. Rahman, and M. F. Hossain, "Classification of Osteosarcoma Tumor from Histological Image Using Sequential RCNN."

[3] D. Anisuzzaman, H. Barzekar, L. Tong, J. Luo, and Z. Yu, "A deep learning study on osteosarcoma detection from histological images," *Biomedical Signal Processing and Control,* vol. 69, p. 102931, 2021.

[4] W. Lan, D. Lai, Q. Chen, X. Wu, B. Chen, J. Liu*, et al.*, "LDICDL: LncRNA-disease association identification based on collaborative deep learning," *IEEE/ACM Transactions on Computational Biology and Bioinformatics,* 2020.

[5] Y. Fu, P. Xue, H. Ji, W. Cui, and E. Dong, "Deep model with Siamese network for viable and necrotic tumor regions assessment in osteosarcoma," *Medical Physics,* vol. 47, pp. 4895-4905, 2020.

[6] J. Zhong, Y. Hu, L. Si, G. Jia, Y. Xing, H. Zhang*, et al.*, "A systematic review of radiomics in osteosarcoma: utilizing radiomics quality score as a tool promoting clinical translation," *European radiology,* vol. 31, pp. 1526-1535, 2021.

[7] S. Y. Jeong, W. Kim, B. H. Byun, C.-B. Kong, W. S. Song, I. Lim*, et al.*, "Prediction of chemotherapy response of osteosarcoma using baseline 18F-FDG textural features machine learning approaches with PCA," *Contrast media & molecular imaging,* vol. 2019, 2019.

[8] H. M. Pereira, M. E. D. Leite, I. R. Damasceno, O. Santos, Luiz Afonso, and M. H. Nogueira-Barbosa, "Machine learning-based CT radiomics features for the prediction of pulmonary metastasis in osteosarcoma," *The British Journal of Radiology,* vol. 94, p. 20201391, 2021.

[9] R. Zhang, L. Huang, W. Xia, B. Zhang, B. Qiu, and X. Gao, "Multiple supervised residual network for osteosarcoma segmentation in CT images," *Computerized Medical Imaging and Graphics,* vol. 63, pp. 1-8, 2018.

[10] J. Dufau, A. Bouhamama, B. Leporq, L. Malaureille, O. Beuf, F. Gouin*, et al.*, "Prediction of chemotherapy response in primary osteosarcoma using the machine learning technique on radiomic data," *Bulletin du cancer,* vol. 106, pp. 983-999, 2019.

[11] K. Makielski, A. J. Donnelly, A. Khammanivong, M. C. Scott, A. R. Ortiz, D. C. Galvan*, et al.*, "Development of an exosomal biomarker signature to detect minimal residual disease in dogs with osteosarcoma using a novel xenograft platform and machine learning," *bioRxiv,* 2021.

[12] S. Wang, H. Jia, and X. J. M. B. E. Peng, "Modified salp swarm algorithm based multilevel thresholding for color image segmentation," vol. 17, pp. 700-724, 2020.

[13] G.-Z. Zhang, Z.-L. Wu, C.-Y. Li, E.-H. Ren, W.-H. Yuan, Y.-J. Deng*, et al.*, "Development of a machine learning-based autophagy-related lncRNA signature to improve prognosis prediction in osteosarcoma patients," *Frontiers in Molecular Biosciences,* vol. 8, 2021.

[14] Y. Deng, W. Yuan, E. Ren, Z. Wu, G. Zhang, and Q. Xie, "A four-methylated LncRNA signature predicts survival of osteosarcoma patients based on machine learning," *Genomics,* vol. 113, pp. 785-794, 2021.

[15] D. Anisuzzaman, H. Barzekar, L. Tong, J. Luo, and Z. Yu, "A Deep Learning Study on Osteosarcoma Detection from Histological Images," *arXiv preprint arXiv:2011.01177,* 2020.

[16] R. Mishra, O. Daescu, P. Leavey, D. Rakheja, and A. Sengupta, "Histopathological diagnosis for viable and non-viable tumor prediction for osteosarcoma using convolutional neural network," in *International Symposium on Bioinformatics Research and Applications*, 2017, pp. 12-23.

[17] W. Chang, Y. Liu, Y. Xiao, X. Yuan, X. Xu, S. Zhang*, et al.*, "A machine-learning-based prediction method for hypertension outcomes based on medical data," *Diagnostics,* vol. 9, p. 178, 2019.